International Journal of Advanced Trends in Engineering and Management
(ISSN 2583-7052)

Vol. V, No. 04, pp. 1-14, April

Densenet-Based Deep Learning Architecture for Multi-Subtype Tracheal Tumor Detection

T. Brinda[1*], Srikanth Mylapalli[3]

[1]Assistant Professor, Department of Computer science and Engineering, Anna University, Tirunelveli, Tamil Nadu, India – 627 007.
[3]Assistant professor, Department of Computer science and Engineering, Tirumala Engineering College, Jonnalagadda, Andhra Pradesh, India – 522 601.
brinda.t@auttvl.ac.in

ABSTRACT: This research presents a DenseNet-based deep learning architecture for detecting multi-subtype tracheal tumors that employs an efficient medical image processing pipeline. The proposed method begins with data collection and progresses through preprocessing processes such as image resizing, contrast enhancement with adaptive gamma correction, noise reduction, and bilateral filtering to improve image quality. The improved images are then segmented using the watershed technique, which efficiently separates tumor locations from surrounding tissues. Critical textural information are retrieved using the Local Binary Pattern (LBP) approach and then classed using the DenseNet model to accurately identify tumor subtypes. The proposed system performs highly with an accuracy of 94.1%, precision of 94.2%, recall of 94.1%, and F1 score of 94.1%, indicating robustness and reliability. The combination of these steps results high accuracy, efficiency, and stability in detecting and categorizing tracheal cancers, allowing for better clinical diagnosis and decision-making.

Keywords: DenseNet, Bilateral filter, Water Shed Segmentation, Local Binary Pattern (LBP).

1. Introduction

Tracheal cancer is a major global health concern. Globalization has a significant impact on the shifting epidemiology of several malignancies, including tracheal carcinoma. This rare but severe cancer has demonstrated differences in incidence and risk variables as a result of increased economic interconnectedness, urbanization, lifestyle changes, and environmental exposures associated with globalization. Changes in global lifestyles, pollution levels, and occupational dangers have all contributed to variations in the patterns and prevalence of tracheal cancer among areas [1]. Primary tracheal malignancies are extremely rare tumors. The most common histological type is squamous cell carcinoma (SCC), followed by adenoid cystic carcinoma (ACC). These two kinds account for over 75% of all primary tracheal malignancies in adulthood. 1, 2 Primary tracheal malignancies other than SCC or ACC are uncommon and have a diverse histological appearance [2]**.** Although the fact that there are various therapy options for tracheal cancer, the condition remains difficult to manage. Therefore, it is necessary to find creative and effective therapy techniques for tracheal cancer. The purpose of this review is to summarize recent advances in nanomedicine-based delivery systems, molecular targeted therapies, image thermal treatment strategies, and immunotherapy approaches for tracheal cancer, with the hope of providing new perspectives and insights into improving treatment outcomes [3].

The preprocessing stage enhances the visual clarity of tracheal medical images by removing noise, adjusting contrast, and using edge-preserving filtering techniques. The median filter is a nonlinear approach for detecting tracheal cancer that removes noise while keeping edges. It replaces each pixel with the median of nearby values, minimizing salt-and-pepper noise and improving tissue visibility for more precise tumor detection. However, it may blur small edges, is less effective against Gaussian noise, and its efficacy is dependent on the window size [4]. In tracheal cancer diagnosis, the mean filter smoothes images and reduces noise by averaging neighboring pixel values. It improves overall clarity but may blur edges, lose fine details, and diminish accuracy in spotting small or low-contrast malignancies [5]. The bilateral filter in tracheal cancer detection reduces noise while conserving edges, improving tumor visibility and image quality. This section covers the preprocessing procedure used to increase image quality and tumor visibility before segmentation.

The segmentation stage isolates tumor regions from normal tracheal tissues, resulting in accurate boundaries for detection and categorization. Otsu thresholding selects the optimal intensity threshold to distinguish tumor regions from normal tracheal tissue by minimizing intra-class variance. It effectively identifies potential cancer spots for future investigation using the DenseNet model. However, it is sensitive to noise and low contrast, which might result in erroneous segmentation when tumor and tissue intensities are comparable [6]. K-means clustering segments tracheal images into groups of pixels with similar intensity or texture to separate tumor spots for DenseNet analysis. It is simple and efficient, but its performance is limited by the number of clusters picked and its sensitivity to low contrast or bad initial cluster selection [7]. Watershed segmentation in tracheal cancer detection segments tumor regions based on intensity gradients, effectively defining borders but frequently resulting in over-segmentation in noisy images. This section demonstrates the method to combine traditional segmentation with deep learning marker creation to achieve precise tumor localization.

The feature extraction stage aims to mathematically represent tumor locations by examining texture and structure patterns in segmented tracheal images.GLCM uses pixel intensity relationships to extract textural information such as contrast, correlation, and homogeneity in order to distinguish tumor regions from normal tissues. It contributes significantly to DenseNet classification but is limited by its sensitivity to noise, rotation, and light fluctuations [8]. The wavelet technique separates tracheal images into numerous frequency subbands in order to obtain precise texture and edge data for accurate tumor diagnosis. Its constraints include the reliance on appropriate wavelet selection and increased computing complexity [9]. The Histogram of Oriented Gradients (HOG) method for tracheal cancer diagnosis computes gradient orientations in confined image regions to extract edge and shape-based information. This procedure aids in the capturing of structural patterns in tumor locations, hence boosting feature input to the DenseNet model. However, it performs badly on low-contrast or fuzzy images since it relies largely on crisp edge information for successful recognition [10]. Local Binary Pattern (LBP) in tracheal cancer diagnosis detects local texture alterations by comparing each pixel to its neighbors, successfully differentiating tumor locations based on surface intensity patterns. The use of multi-scale and extended LBP improves resistance to fluctuations in lighting and orientation, resulting in highly discriminative features for DenseNet classification.

The classification step uses the DenseNet deep learning architecture to distinguish tracheal tumor subtypes based on retrieved LBP features.

MobileNetV2, a lightweight deep learning model, is frequently utilized for image classification tasks in medical imaging, such as tracheal tumor identification. Its efficiency, due to lower computational resources, allows for real-time processing on mobile and edge devices, making it perfect for contexts with limited resources. However, its limits in tumor detection include lower accuracy when compared to larger models, particularly in complicated or subtle tumour characteristics [11]. ResNet-18, a deep residual network, is frequently utilized in medical image analysis for tasks such as tracheal tumor detection because of its capacity to effectively train deeper architectures using residual connections. It specializes at capturing complicated details, which improves its accuracy in detecting cancers in tracheal images. However, ResNet-18 is still susceptible to issues with high processing demands, rendering it unsuitable for real-time applications or mobile devices [12]. SqueezeNet is a small convolutional neural network that achieves good accuracy with much less parameters, making it ideal for detecting tracheal tumors in resource-constrained environments. Its "fire modules" compress and extend feature maps efficiently, lowering model size while retaining good performance. However, its lightweight construction may limit its ability to capture fine-grained or complicated tumor features, reducing detection accuracy [13]. DenseNet improves tracheal cancer diagnosis by encouraging efficient feature reuse and strong gradient flow, resulting in increased accuracy in spotting subtle tumor patterns. The DenseNet-based approach thus allows for rapid and exact subtype identification, which supports early and effective clinical decision-making.

1.1 Realed Works

Svetlana Valjarevic *et al* (2025) [14] have developed SVM-based detection of nuclear changes in laryngeal cancer using fractal and run-length features. A Support Vector Machine (SVM) employs hyper planes to identify nuclear features in laryngeal cancer based on fractal and run-length matrix indicators, efficiently discriminating between normal and abnormal nuclei. It works well with high-dimensional data and small sample sizes, making it ideal for comprehensive histopathology examination. However, with large datasets, SVM can be computationally costly and is sensitive to kernel selection and parameter adjustment. Furthermore, it may struggle with overlapping classes or noisy images, lowering classification accuracy.

Iman Akour *et al* (2025) [15] have proposed Thyroid Cancer Recurrence Prediction using Tribal Intelligence and XGBoost. The system works by modelling intelligent tribal behavior to explore and develop predictive features, which improves the accuracy and stability of recurrence identification. It uses XGBoost's gradient boosting algorithm to effectively handle nonlinear interactions and complex medical data. However, disadvantages include the possibility of overfitting on limited datasets, significant processing costs during optimization, and poor interpretability of model decisions, all of which may have an impact on clinical applicability.

Sakineh *et al* (2023) [16] have implemented Voice Evaluation in Nonlaryngeal Head and Neck Cancer Patients Using Binary Logistic Regression. The model works by investigating the correlations between clinical, acoustic, and perceptual characteristics to predict post-treatment voice dysfunction. This method allows for both objective and subjective assessments of vocal results, facilitating data-driven clinical evaluation. However, constraints include the model's reliance on sample size and data quality, potential bias from subjective measurements, and its inability to capture complicated nonlinear interactions between affecting factors.

Cherif *et al* (2025) [17] have developed EMD-Based Mel-Spectrograms and AlexNet for Detecting Laryngeal Pathology. The proposed method use Empirical Mode Decomposition (EMD) to extract intrinsic voice signal properties and generate Mel-spectrograms that capture both the temporal and frequency characteristics of speech. To automatically categorize and detect laryngeal diseases, the AlexNet deep learning model is applied to these spectrograms. This method improves diagnosis accuracy by combining adaptive signal decomposition with deep feature learning. However, shortcomings include EMD's computational complexity, potential overfitting on short datasets, and lower performance in noisy or low-quality voice recordings.

Hongpeng *et al* (2025) [18] have proposed Thyroid Cancer Subtype Classification Using EfficientNetB0. The proposed model uses EfficientNetB0 to classify thyroid cancer subtypes from medical images while efficiently balancing network depth, width, and resolution. The approach collects precise visual data and improves classification accuracy while being computationally efficient. Its lightweight architecture allows for faster training and improved generalization on restricted medical datasets. Nevertheless constraints include sensitivity to data imbalance, potential overfitting with small sample sizes, and decreased interpretability of deep learning conclusions in clinical settings.

1.2 Objectives

- To collect high-quality tracheal medical images for precise tumor detection.
- To enhance the photos, resize them, apply adaptive gamma correction, reduce noise, and use bilateral filtering.
- To efficiently separate tracheal regions, use the watershed method to isolate tumor-affected areas.
- To extract relevant textural and structural information from segmented images, use the Local Binary Pattern (LBP) approach.
- To increase diagnostic accuracy, use the DenseNet deep learning network to classify and identify various tracheal tumor subtypes.

2. Proposed System Description

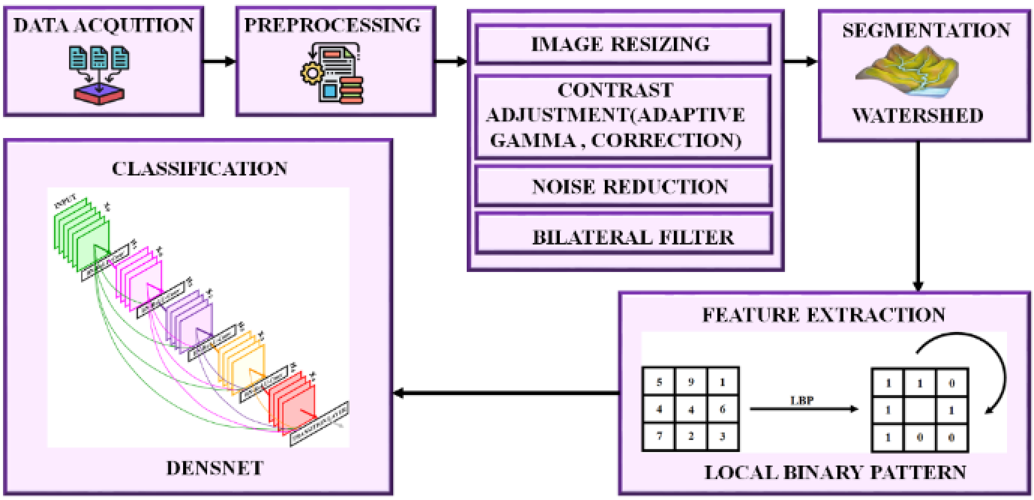

Figure 1: *Block diagram of proposed system*

Figure 1 shows the proposed framework for multi-subtype tracheal tumor identification begins with data acquisition, which involves collecting medical imaging data from the trachea, such as CT or MRI scans. The images go through a preprocessing stage that includes image resizing for uniformity, contrast modification with adaptive gamma correction to improve visibility, noise reduction, and bilateral filtering to smooth the image while retaining critical edges. The preprocessed images are then segmented with the watershed method, which accurately distinguishes the tumor location from the surrounding tissues. After segmentation, the LBP approach is used to extract critical texture and intensity information for tumor characterisation. Finally, these collected features are entered into a DenseNet-based classification model, which efficiently recognizes and classifies various tracheal subtypes. This integrated approach improves diagnostic precision, resulting in more reliable and efficient diagnosis of tracheal anomalies.

3. Proposed System Modelling

3.1 Preprocessing By Bilateral Filter

Image processing for tracheal cancer detection is examining medical images, such as CT or MRI scans, to find aberrant tissue growth or structural abnormalities. To increase the visibility of tumor locations and improve diagnostic accuracy, preprocessing techniques such as images scaling, contrast enhancement, noise reduction, and bilateral filtering (BF) are used.

The luminance profile $I(x)$ is defined on a discrete domain $\Omega \subseteq \mathbb{Z}_n$, with each $x \in \Omega$ representing a pixel or voxel. The bilateral filter (BF) produces $U(x)$, a weighted average of surrounding pixel values, which is defined as:

$$U(x) = \frac{N(x)}{D(x)} \tag{1}$$

The BF computes weighted sums based on spatial distance $\left(g_{\sigma 1}(x-y)\right)$ and intensity differences$\left(w_{\sigma 2}\left(I(x)-I(y)\right)\right)$, with σ1 and σ2 determining spatial and intensity sensitivity, respectively. This enables the filter to efficiently reduce image noise while maintaining the distinct edges of tumor margins and tracheal borders.

Preserving edge features is critical in tracheal cancer detection because tiny intensity differences frequently suggest tumor borders or abnormal tissue development. The bilateral filter effectively decreases background and scanning noise while preserving essential edge information, making it ideal for improving tumor visibility in medical imaging.

Image scale and contrast adjustment: While standardizing image dimensions enhances computing efficiency for deep learning models, it may also result in the loss of subtle anatomical details. Adaptive gamma correction dynamically increases image contrast to compensate for uneven illumination, showing tiny differences in tracheal tissue densities that could indicate early-stage malignancies.

The bilateral filter's ability to reduce noise while preserving sharp edges makes it an important preprocessing step for detecting tracheal malignancy. The $\sigma 2$ parameter balances noise reduction with edge retention. Higher values lower noise but may significantly soften tumor features. However, bilateral filtering is computationally demanding since it processes a vast area surrounding each pixel. To address this, acceleration methods such as domain transform filtering and bilateral grid filtering are used to minimize computational complexity, allowing for faster image processing appropriate for real-time diagnostic systems.

A strong preprocessing framework for tracheal cancer detection is developed by combining image scaling, adaptive gamma correction, noise reduction, and bilateral filtering. Fine-tuning the bilateral filter settings guarantees precise edge preservation, while computational optimization approaches enable for fast analysis of both static and real-time tracheal imaging data.

3.2 Watershed Segmentation

Accurate segmentation is critical in tracheal tumor detection because it distinguishes tumor boundaries from surrounding tissues. Traditional region-growing algorithms, such as the watershed algorithm, necessitate trustworthy object markers, which are frequently dependent on prior knowledge, such as the number of tumor regions, image texture features, or approximate tumor locations. Because these factors vary widely between patients, deep learning-based segmentation offers a more robust and automated solution for exact marker identification.

The proposed tracheal tumor detection framework extracts Local Binary Pattern (LBP) features from tracheal CT or MRI images to capture texture variations found in tumor tissues. These LBP characteristics are then utilized to train a DenseNet classifier, indicated as h_{marker}, which produces precise tumor object markers. To ensure that identified markers are totally within tumor borders, the classifier is trained using morphologically degraded ground-truth labels, given as

$$L_{eroded} = L \oslash B \tag{2}$$

Where L_{eroded} represents erosion of the label image L caused by a structural feature B. The DenseNet-based marker identification classifier, P_{marker} is given by:

$$P_{marker}(i,j) = P[L_{eroded}(i,j)| + (i,j)] \tag{3}$$

$$P_{marker}(i,j) = h_{marker}\big(f(i,j)\big) \tag{4}$$

Here, $f(i,j)$ is the feature vector at pixel location (i,j) obtained from LBP descriptors. The classifier h_{marker} predicts tumor marker probabilities, whereas h_{region} and p_{region} represent the DenseNet model trained on standard ground truth and its probability map, respectively. Experimental results reveal that hmarker produces more precise and accurate tumor markers than basic probability thresholding of p_{region}.

The following phase is to build the topological surface for the watershed algorithm after defining p_{region}, which is used to define tumor background boundaries, and P_{marker}, which is used to identify tumor cores. DenseNet-generated probability maps serve as adaptive topological surfaces in place of the raw picture gradient. Using the inverted probability map 1−Pregion guarantees that regions with higher tumor probability are segmented first because the highest intensity values within p_{region} indicate pixels most likely belonging to tumor regions. Using hard thresholding, regional minima are determined based on the marker locations taken from P_{marker}.

This integrated method improves tumor border localization, reduces over-segmentation, and produces precise tracheal tumor region delineation by combining LBP-based feature extraction, DenseNet classification, and watershed segmentation.

3.3 Feature Extrtaction Based on Local Binary Pattern

The LBP operator is widely used as an extraction technique in medical image analysis, including the detection of tracheal tumors. LBP extracts texture characteristics by comparing each pixel to its 3×3 neighborhood and encodes the result as a binary number. The histogram of these binary values thus functions as a reliable texture descriptor, capturing local patterns in the image. This approach aids in the identification of crucial tumor traits such as shape, edges, and texture changes, which are necessary for distinguishing various tumor subtypes. Traditional LBP, on the other hand, is sensitive to changes in illumination and viewpoint, both of which are common in medical imaging.

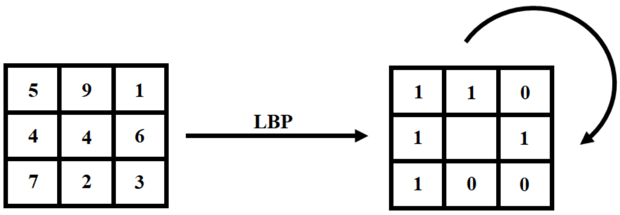

Figure 2: *Local binary pattern*

To improve LBP feature extraction, a multi-scale LBP technique is used. Instead of a fixed 3x3 neighborhood, circular neighborhoods with bilinear interpolation are employed, allowing for adjustable neighborhood sizes. This allows for extraction of textural features at various scales, capturing both coarse and fine details in the tracheal tissue. Summing the histograms from different scales rather than concatenating them keeps the feature vector consistent in length while keeping important multi-scale information. The multi-scale LBP improves the ability to identify tiny texture differences, which are critical for distinguishing tumor subtypes.

Traditional LBP only captures first-order texture information; however, extended LBP is used to represent local texture changes more accurately. The extended version entails creating derivative images that capture the rate of change in intensity values, so providing additional dynamic information about the texture. Using Sobel filters, we compute the horizontal and vertical gradients, yielding two types of derivative images:

Gradient magnitude image

$$|\nabla I| = \sqrt{(h_x \otimes I)^2 + \left(h_y \otimes I\right)^2} \quad (5)$$

This image focuses on locations with strong texture changes, such as tumor borders and boundaries.

Gradient direction image

$$\psi(\nabla \mathrm{I}) = arctan\left(\frac{(h_y \otimes I)}{(h_x \otimes I)}\right) \quad (6)$$

The direction image records the orientation of texture changes, which provides information on the tumor's shape and orientation.

By using the LBP operator on both the original and gradient magnitude images, they attain richer, more informative texture features. This provides a more detailed image of the texture of the tracheal tumor and is critical for discriminating between different tumor subtypes, such as benign or malignant.

In this study, LBP is employed as a feature extraction technique to detect multi-subtype tracheal tumors. The combination of multi-scale LBP and extended LBP (which include gradient magnitude and direction) improves texture representation of tracheal tissues greatly. These enhanced LBP characteristics help capture both static and dynamic texture fluctuations, which is useful for discriminating across tumor subtypes. The proposed approach exhibits the ability of LBP to improve the accuracy of tracheal tumor classification in medical image analysis.

3.4 Classfication Based on Densenet

DenseNet is a deep learning architecture in which all layers are directly connected, allowing for efficient information flow. This connectedness is especially useful for detecting tracheal tumors since it ensures that each layer benefits from the information learnt by preceding layers. DenseNet has fewer parameters than typical CNNs and reduces overfitting, which is important when working with limited medical datasets. The model works well in evaluating CT or MRI scans of the trachea to detect tumor borders and textural variations.

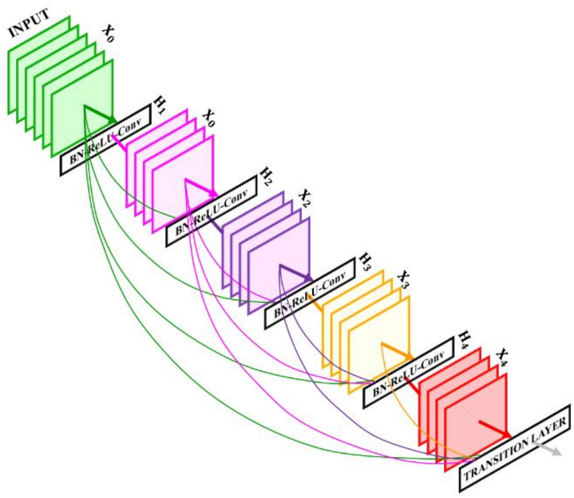

Figure 3: *DenseNet classification*

Consider an input image $(x_\circ)$ representing a tracheal scan, which is relayed via N levels in the network. Each layer uses a nonlinear transformation $F_n(\cdot)$, which takes the feature maps from all previous layers $(0\ to\ n-1)$ as input. Layer n produces the following output:

$$x_n = F_n([x_\circ, \dots, x_{n-1}]) \quad (7)$$

Where $F_n(\cdot)$ consists of 3×3 convolution (Conv), Rectified Linear Units (ReLU), and Batch Normalization (BN) operations, enabling network to capture crucial properties including tumor texture and shape.

In DenseNet, transition layers employ 3×3 convolutions, BN, and ReLU. 1x1 convolutions and 2x2 average pooling are used to down sample layers with varying feature map sizes. To extract fundamental information, the network begins with a 7x7 convolution layer. Following the last dense block, the image is classified into predetermined tumor subtypes using Global Average Pooling (GAP) and a Softmax classifier.

Convolution techniques preserve pixel associations while learning the features of the image. ReLU activation, which adds nonlinearity to catch intricate patterns, comes after these procedures. The definition of the ReLU function is:

$$f(x_\circ) = max(0.x_\circ) \tag{8}$$

allowing model to focus on the most significant features of the image.

Pooling operations, such as max and average pooling, lower the dimensionality of feature maps. Max pooling focuses on the greatest numbers, whereas average pooling computes the mean, decreasing noise. In the final phase, Global Average Pooling (GAP) averages each feature map before passing the result to the Softmax layer, which identifies the image as one of the tumor subtypes.

Finally, the DenseNet-based design successfully captures and classifies complicated information in tracheal tumor images. The model's use of convolutions, pooling, and nonlinear functions allows it to detect small differences in tumor shape, texture, and borders, which improves tumor subtype categorization for accurate diagnosis and therapy.

4. Result and Discussion

The proposed DenseNet-based model performed well in identifying and classifying tracheal cancer subtypes, with an accuracy of 94.1%, a precision of 94.2%, a recall of 94.1%, and an F1 score of 94.1%. These results outperform previous techniques and are confirmed by strong AUC values, indicating that the model is reliable and useful for clinical usage.

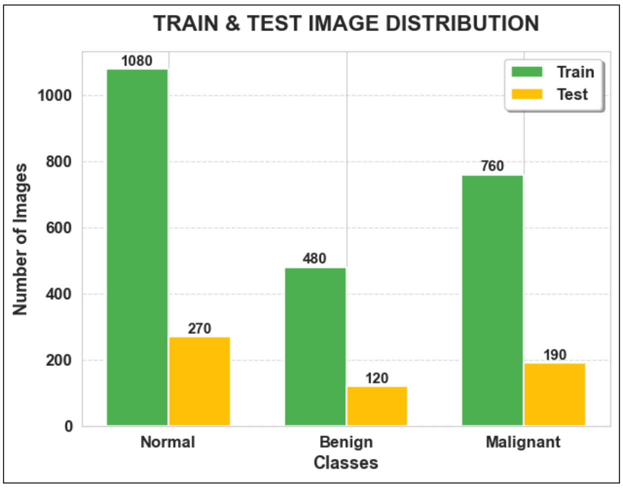

Figure 4: *Train & Test image distribution*

Figure 4 shows the distribution of images across three categories (Normal, Benign, and Malignant) divided between the training and testing datasets. The chart demonstrates that the Normal class has the most images in training set (1080), whereas the testing set only has 270 images. The Benign class contains 480 images in training set and 120 in the testing set, whereas the Malignant class contains 760 images in the training set and 190 in the testing set. This distribution demonstrates the differences in images count between the training and testing datasets for each class.

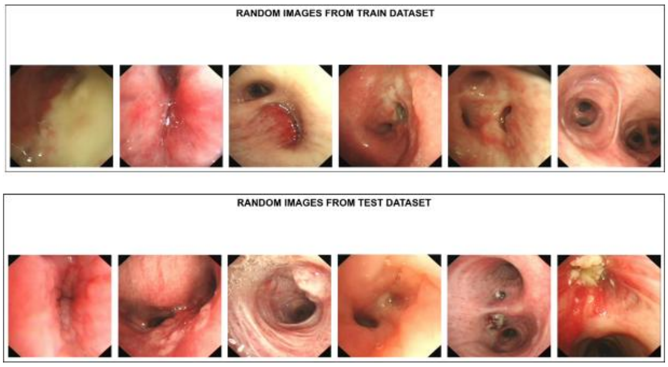

Figure 5: *Random images from Train and Test Datasets*

Figure 5 represents that the random images from the training and test datasets. The top row displays images from training dataset, while the bottom row contains images from test dataset. The images provide a visual representation of the data utilized for model training and testing, highlighting differences in the medical conditions under consideration. These images appear to be medical in origin, possibly related to eye examination or diagnostics, and depict various types of disorders found in the collection.

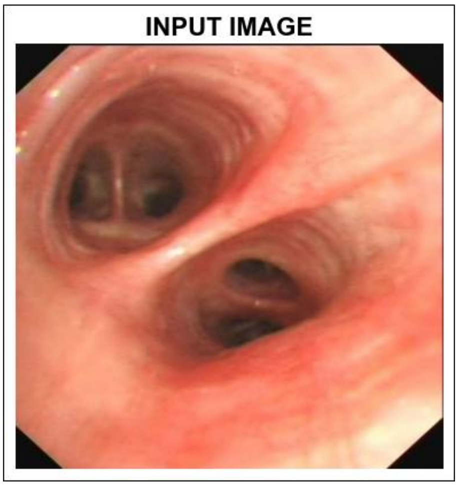

Figure 6: *Input image*

Figure 6 indicates an example of an input image for analysis. The image looks to be an endoscopic view of a body portion, most likely obtained during a medical diagnostic operation. It is labelled as the "Input Image," implying that it is the raw data provided into a system or model for processing, categorization, or further investigation in medical study.

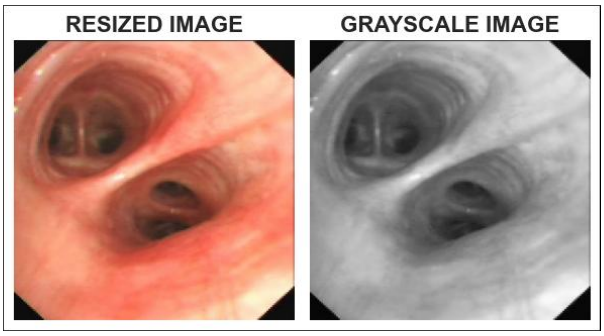

Figure 7: *Resize and grayscale conversion of tracheal image*

Figure 7 shows the preprocessing scaled version, which ensures uniform dimensions for computational efficiency in model training. The right image depicts the grayscale-converted result, which decreases color complexity and highlights intensity changes that are critical for spotting aberrant tissue regions in tracheal cancer investigation.

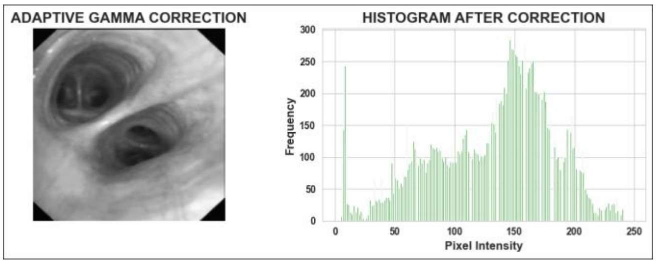

Figure 8: *Adaptive gamma correction and histogram analysis*

Figure 8 indicates the adaptive gamma correction is used to enhance tracheal images. The left image shows the improved contrast output after rectification, which emphasizes finer structural details of the tracheal walls. The right histogram shows the redistribution of pixel intensities, indicating balanced brightness and better visual clarity, which are required for accurate tumor region analysis.

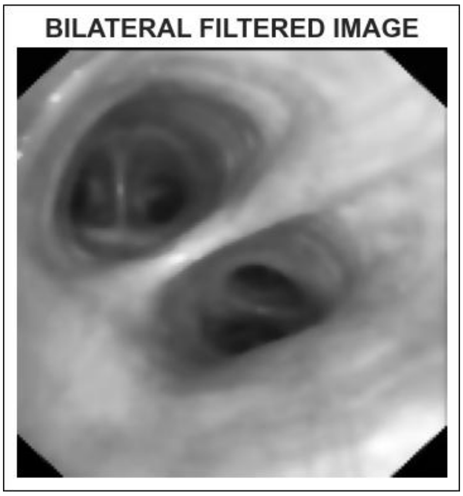

Figure 9: *Bilateral filter tracheal image*

Figure 9 represents the tracheal image after applying a bilateral filter, which efficiently lowers noise while keeping important edge details. The filtering improves tissue smoothness while preserving the anatomical boundaries required for effective tracheal tumor segmentation and classification in the deep learning workflow.

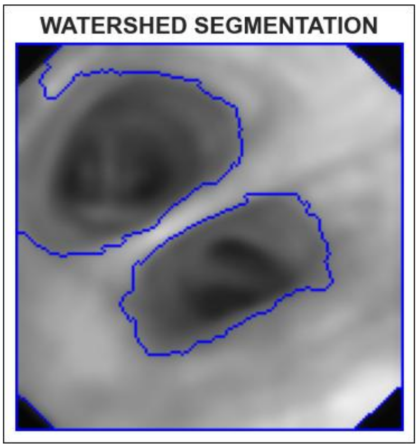

Figure 10: *Watershed segmentation of tracheal image*

Figure 10 indicates the segmented tracheal areas acquired using the watershed segmentation technique. The approach accurately delineates tumor boundaries by separating overlapping structures based on gradient intensity, improving the precision of lesion localization for tracheal cancer diagnosis.

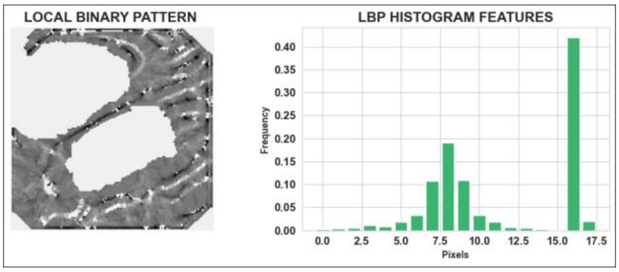

Figure 11: *Local binary patter (LBP) and its histogram features*

Figure 11 shows the Local Binary Pattern (LBP) texture descriptor and its associated histogram features. The image on the left demonstrates the results of using the Local Binary Pattern approach to highlight textures by encoding pixel intensity differences. On the right, the histogram shows the frequency of various LBP values (in terms of pixel intensity), with peaks indicating the image's dominating patterns. The histogram indicates how frequently various LBP codes appear, which helps with texture analysis, pattern recognition, and classification tasks.

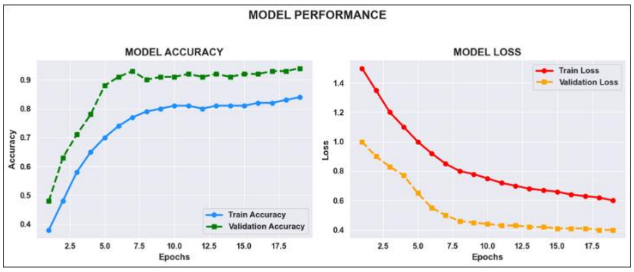

Figure 12: *Model performance accuracy and loss curve*

Figure 12 indicates performance of a machine learning model while training. The Model Accuracy plot on the left depicts how the training and validation sets' accuracy changes over time. As the model learns, its accuracy improves, but it eventually reaches a plateau as it generalizes. On the right, the Model Loss plot shows the loss values for both the training and validation sets. The loss lowers over time, demonstrating that the model improves as it trains. These graphs are helpful for analysing the model's learning progress and detecting whether it is overfitting or under fitting.

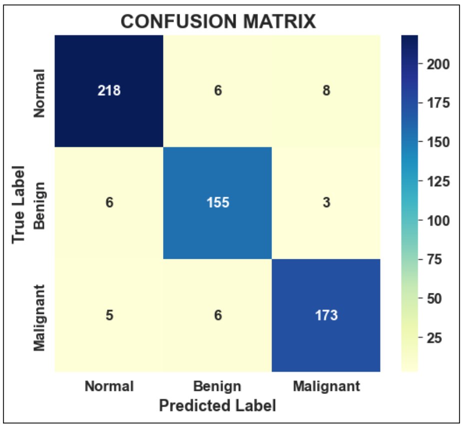

Figure 13: *Confusion matrix for classification performance*

Figure 13 represents the confusion matrix used to assess the performance of a classification model across three classes: normal, benign, and malignant. The matrix shows number of correct and incorrect predictions for each class, with diagonal entries representing correctly categorized samples and off-diagonal elements denoting misclassification. The high values along the diagonal indicate that the model distinguishes well across the three groups, exhibiting excellent overall classification accuracy.

Table 1: *Model Evaluation Metrics*

Performance Metrics	
Accuracy	94.1%
Precision	94.2%
Recall	94.1%
F1 score	94.1%

Table 1. shows the model's performance was evaluated using key metrics listed in the Performance Metrics Summary table. It had an accuracy of 94.1%, indicating a high rate of right predictions. The precision of 94.2% indicates that the majority of positive predictions were correct, while the recall of 94.1% displays the model's ability in detecting true positives. The F1 score of 94.1% demonstrates a solid mix of precision and recall, validating the model's overall dependability and consistency.

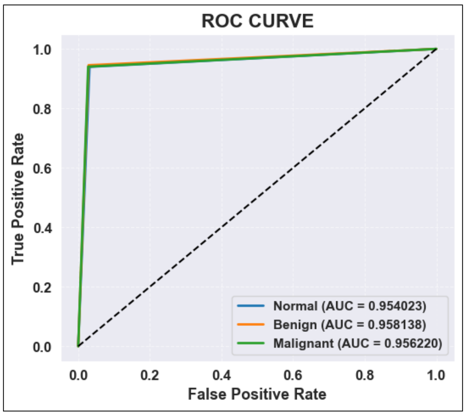

Figure 14: *ROC curve for model classification performance*

Figure 14 represents the model’s ability to distinguish between Normal, Benign, and Malignant classes. With AUC values of 0.9540, 0.9581, and 0.9562, respectively, the model demonstrates excellent classification performance and strong discriminative power.

Table 2: *Comparison of model accuracy with existing methods*

Method	Accuracy
proposed	94.1%
CPTG[12]	72.8%
EPTS[14]	83.4%

Table 2. compares the proposed model's accuracy to existing approaches like CPTG [12] and EPTS [14]. The proposed model had the maximum accuracy of 94.1%, beating CPTG (72.8%) and EPTS (83.4%), demonstrating superior performance and effectiveness in making more accurate predictions.

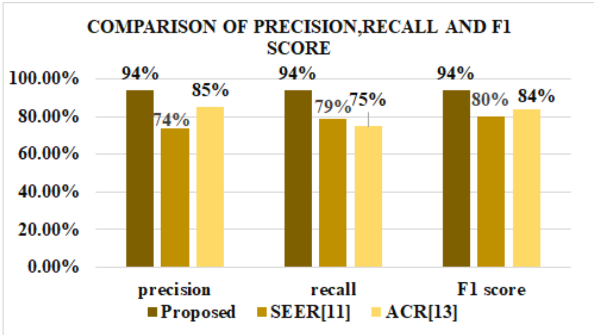

Figure 15: *Comparison of precision, recall and F1 score across different methods*

Figure 15 denotes the proposed model's precision, recall, and F1 score to existing techniques, SEER [11] and ACR [13]. The proposed approach obtains the highest values across all three criteria, with precision, recall, and F1 scores of roughly 94%, beating SEER and ACR, which have lower scores. These findings show the predicted model's improved classification accuracy and dependability.

5. Conclusion

In conclusion, the proposed DenseNet-based deep learning framework is an excellent and dependable method for detecting multi-subtype tracheal cancer. The model achieves excellent classification performance with 94.1% accuracy, 94.2% precision, 94.1% recall, and 94.1% F1 score, thanks to a well-structured pipeline that includes advanced preprocessing, watershed method segmentation, and LBP-based feature extraction. These findings support the model's greater capacity to reliably identify tumor subtypes in comparison to previous techniques. The system's high accuracy, robustness, and efficiency make it an important tool for assisting physicians in early diagnosis and decision-making, ultimately contributing to better patient care and advances in computer-aided cancer detection.

Reference

1. Mengwei Zhang; Weiqiu Jin; Yu Tian; Hongda Zhu; Ningyuan Zou; Yunxuan Jia; Long Jiang; Jia Huang; Yingjie Hu; Qingquan Luo, Year: 2023, “Cancer burden variations and convergences in globalization: a comparative study on the tracheal, bronchus, and lung (TBL) and liver cancer burdens among WHO regions from 1990 to 2019”, Journal of Epidemiology and Global Health, Vol: 13, No: 4, pp. 696-724.
2. Aleksandra Piórek; Adam Płużański; Paweł Teterycz; Sylwia Tabor; Kinga Winiarczyk; Magdalena Knetki-Wróblewska; Dariusz M. Kowalski; Maciej Krzakowski, Year: 2024, “Clinicopathological characteristics of patients with primary tracheal tumors: Analysis of eighty-nine cases”, Thoracic Cancer, Vol: 15, No: 11, pp. 878-883.
3. Yuting Li; Bingshuo Yan; Shiming He, Year: 2023, “Advances and challenges in the treatment of lung cancer”, Biomedicine & Pharmacotherapy, Vol: 169, pp. 115891.
4. Sarah Zuhair Kurdi; Mohammed Hasan Ali; Mustafa Musa Jaber; Tanzila Saba; Amjad Rehman; Robertas Damaševičius, Year: 2023, “Tumor Classification Using Meta-Heuristic Optimized Convolutional Neural Networks”, Journal of Personalized Medicine, Vol: 13, No: 2, pp. 181.
5. Harinahalli Lokesh Gururaj; N. Manju; A. Nagarjun; VN Manjunath Aradhya; Francesco Flammini, Year: 2023, “DeepSkin: A Deep Learning Approach for Skin Cancer Classification”, in IEEE Access, Vol: 11, pp. 50205-50214.
6. Javeed, Muhammad Awais, Muhammad Arslan Ghaffar, Muhammad Awais Ashraf, Nimra Zubair, Ahmed Sayed M. Metwally, Elsayed M. Tag-Eldin, Patrizia Bocchetta, Muhammad Sufyan Javed, and Xingfang Jiang, Year: 2023, “Lane Line Detection and Object Scene Segmentation Using Otsu Thresholding and the Fast Hough Transform for Intelligent Vehicles in Complex Road Conditions”, Electronics, Vol: 12, No: 5, pp. 1079.
7. Seyed Mahdi Miraftabzadeh; Cristian Giovanni Colombo; Michela Longo; Federica Foiadelli, Year: 2023, “K-Means and Alternative Clustering Methods in Modern Power Systems”, in IEEE Access, Vol: 11, pp. 119596-119633.
8. Ganesha Prasad; Vijay Srinivas Gaddale; Raghavendra Cholpadi Kamath; Vishwanatha Jampenahalli Shekaranaik; Srinivasa Padubidri Pai, Year: 2024, “A study of dimensionality reduction in GLCM feature-based classification of machined surface images”, Arabian Journal for Science and Engineering, Vol: 49, No: 2, pp. 1531-1553.
9. Ning You; Libo Han; Daming Zhu; Weiwei Song, Year: 2023, “Research on Image Denoising in Edge Detection Based on Wavelet Transform. Appl. Sci., Vol. 13, pp. 1837.
10. Binod Bhattarai; Ronast Subedi; Rebati Raman Gaire; Eduard Vazquez; Danail Stoyanov, Year: 2023, “Histogram of oriented gradients meet deep learning: A novel multi-task deep network for 2D surgical image semantic segmentation”, Medical Image Analysis, Vol: 85, pp. 102747.
11. Wei Shi; Yanhong Ning; Xin Liu; Hang Liu; Chunjuan Zhao; Liyun Wu, Year: 2024, “Prognostic factors and constructing a nomogram in tracheal cancer patients treated with surgical

intervention: A study based on SEER database", Medicine, Vol: 103, No: 1, pp. e36787.

12. J. X. Zhou; P. Ma; M. L. Bao; J. L. Tang; Z. G. Zou; H. X. Li, Year: 2025, "Clinicopathologic features with pulmonary and tracheal glomus tumor: report of 8 cases", Zhonghua Zhong Liu Za Zhi, Vol: 47, No: 4, pp. 349-355.
13. Brent P. Little; Christopher M. Walker; Tami J. Bang; Anupama G. Brixey; Jared D. Christensen; Jose De Cardenas; Stephen B. Hobbs; A. Klitzke; R. Madan; F. Maldonado; M.B. Marshall, Year: 2024, "ACR Appropriateness Criteria® Tracheobronchial Disease", Journal of the American College of Radiology, Vol: 21, No: 11, pp. S518-S533.
14. Hassan Fahmi Alkhars; Turki Al Muhaimid; Fatmah Al Abdulwahid; Maha A. Alharbi, Year: 2023, "Endoscopic excision of primary tracheal schwannoma: a case report", The American Journal of Case Reports, Vol: 24, pp. e939823-1.
15. Zainab Riaz; Bangul Khan; Saad Abdullah; Samiullah Khan; Md Shohidul Islam, Year: 2023, "Lung Tumor Image Segmentation from Computer Tomography Images Using MobileNetV2 and Transfer Learning", Bioengineering, Vol: 10, No: 8, pp. 981.
16. Olayemi David Olalekan; Rumu Yusuf Emmanuel; Ibrahim Umar, Year: 2024, "CANCER DETECTION AND CLASSIFICATION THROUGH TRANSFER LEARNING WITH RESNET18-BASED CONVOLUTIONAL NEURAL NETWORK", Journal of Institutional Research, Big Data Analytics and Innovation, Vol: 1, No: 1, pp. 76-85.
17. Anas Bilal; Ali Alkhathlan; Faris A. Kateb; Alishba Tahir; Muhammad Shafiq; Haixia Long, Year: 2025, "A quantum-optimized approach for breast cancer detection using SqueezeNet-SVM", Scientific Reports, Vol: 15, No: 1, pp. 3254.
18. Svetlana Valjarević; Milan B. Jovanović; Pantić Jovana Paunović; Igor Pantić, Year: 2025, "A novel support vector machine learning approach using fractal and run-length matrix indicators for identifying nuclear changes in laryngeal cancer", MEDICINSKA IS RA I AN A, pp. 41.
19. Mohanad A. Deif; Iman Akour; Mohamed Elhoseny, Year: 2025, "Optimizing Thyroid Cancer Recurrence Prediction Using Tribal Intelligent Evolution and XGBoost: Toward Enhanced Clinical Decision Support", Informatics in Medicine Unlocked, pp. 101702.
20. Sakineh Bagherzadeh; Daryoush Shahbazi-Gahrouei; Farhad Torabinezhad; Seied Rabi Mehdi Mahdavi; Pedram Fadavi; Soraya Salmanian, Year: 2023, "Binary logistic regression modeling of voice impairment and voice assessment in iranian patients with nonlaryngeal head-and-neck cancers after chemoradiation therapy: objective and subjective voice evaluation", Journal of Medical Signals & Sensors, Vol: 13, No: 1, pp. 40-48.
21. Sofiane Cherif; Abdelhafid Kaddour; Abdelmoudjib Benkada; Said Karoui, Year: 2025, "Detection of Laryngeal Pathologies from Voice using EMD-based Mel-Spectrograms and Scalograms with AlexNet", Measurement Science Review, Vol: 25, No: 5, pp. 276-283.
22. Hongpeng Guo; Junjie Zhang; You Li; Xinghe Pan; Chenglin Sun, Year: 2025, "Advanced pathological subtype classification of thyroid cancer using efficientNetB0", Diagnostic Pathology, Vol: 20, No: 1, pp. 28.
23. Lifeng Yin; Pujiang Hong; Guanghai Zheng; Huayue Chen; Wu Deng, Year: 2022, "A novel

image recognition method based on DenseNet and DPRN", Applied Sciences, Vol. 12, No: 9, pp. 4232.